

Learning Nonautonomous Systems via Dynamic Mode Decomposition

Hannah Lu^{a,b,1}, Daniel M. Tartakovsky^{c,*}

^a*Department of Aeronautics and Astronautics, Massachusetts Institute of Technology, Cambridge, MA 02139, USA*

^b*Department of Civil and Environmental Engineering, Massachusetts Institute of Technology, Cambridge, MA 02139, USA*

^c*Department of Energy Science and Engineering, Stanford University, Stanford, CA 94305, USA*

Abstract

We present a data-driven learning approach for unknown nonautonomous dynamical systems with time-dependent inputs based on dynamic mode decomposition (DMD). To circumvent the difficulty of approximating the time-dependent Koopman operators for nonautonomous systems, a modified system derived from local parameterization of the external time-dependent inputs is employed as an approximation to the original nonautonomous system. The modified system comprises a sequence of local parametric systems, which can be well approximated by a parametric surrogate model using our previously proposed framework for dimension reduction and interpolation in parameter space (DRIPS). The offline step of DRIPS relies on DMD to build a linear surrogate model, endowed with reduced-order bases (ROBs), for the observables mapped from training data. Then the offline step constructs a sequence of iterative parametric surrogate models from interpolations on suitable manifolds, where the target/test parameter points are specified by the local parameterization of the test external time-dependent inputs. We present a number of numerical examples to demonstrate the robustness of our method and compare its performance with deep neural networks in the same settings.

Keywords: data-driven learning; nonautonomous systems; manifold interpolations

1. Introduction

With the rapid advances in modern machine learning algorithms and the increasing availability of observational data, there have been growing developments in data-driven learning of complex systems. Various regression techniques [1, 2] use a proposed dictionary, comprising plausible spatial and/or temporal derivatives of a state variable, to “discover” the governing equations from observations. Examples of such numerical methods include sparse identification of nonlinear dynamical systems [3], Gaussian process regression [4], DMD with dictionary learning [5, 6, 7] and deep neural networks (DNNs) [8, 9, 10, 11]. Alternatively, a surrogate (aka reduced-order) model can be constructed from data in a dictionary/equation-free fashion. In this context, DMD can be used to construct an optimal linear approximation model for the unknown system [12] and to learn the unknown dynamics of chosen observables, rather than of the state itself [13]. The latter is accomplished by utilizing the Koopman operator theory [14] in order to construct linear models on the observable space, instead of seeking for nonlinear models on the state space [15]. Likewise, DNN can be used to build nonlinear surrogate models for ODEs [16, 10] and PDEs [17, 18, 19].

Nonautonomous systems have increased complexity as they describe the dynamic behaviors of physical laws due to temporal variations of system parameters, sources term, boundary conditions and etc. Learning such systems from data is extremely challenging as the model has to differentiate the forces driven by internal dynamics from the forces driven by the external factors or inputs that vary with time.

*Corresponding author

Email address: tartakovsky@stanford.edu (Daniel M. Tartakovsky)

¹email: hannahlu@mit.edu

Several studies have explored the application of data-driven methods for learning nonautonomous systems in the context of control and optimization [20, 21, 22, 23]. These methods, however, rely on a fixed structure of time-independent Koopman operator and separated time-dependent forcing/control term. More recently, a time-dependent Koopman operator framework was introduced to nonautonomous dynamical systems in [24]. This extension introduces time-dependent eigenfunctions, eigenvalues and modes of the nonautonomous Koopman operator. Further developments along this line of research include multi-resolution DMD with multiple time scale decomposition [25], spatiotemporal pattern extraction [26], delay-coordinate maps [27]. However, these methods only apply to nonautonomous systems within certain categories (e.g., periodic and quasi-periodic) and/or require special analytic tools (e.g., rescaling) and particular knowledge about the system properties. Meanwhile, there remains numerical challenges in accurate and efficient computations of the nonautonomous Koopman operator spectrum. Online DMD and weighted DMD [28] are developed to recover the approximations of time-dependent Koopman eigenvalues and eigenfunctions. These methods require large amount of data to capture the variations in the Koopman operator in each time window and an intrinsic error is introduced when the DMD method with the state observables is applied, which is further studied and analyzed in [29].

Instead of approximating the time-dependent Koopman operator, our framework transforms learning of nonautonomous systems into learning of locally parameterized systems. This transformation was first used in [30] for recovering unknown nonautonomous dynamical systems based on deep neural networks. The local parameterization of the external time-dependent inputs is defined over a set of discrete time instances and conducted using a chosen local basis over time. The resulting piecewise local parametric systems in each time interval can be learned via our previous framework DRIPS [31]. Once the local surrogate model is successfully constructed from training data, predictions of different initial conditions and time-dependent external inputs can be made by iterative computation of the interpolated parametric surrogate models over each discrete time instances. Our framework serves as a more data-efficient alternative to the DNN based learning method [30] as further studied in numerical experiments.

The remainder of the paper is organized as follows. The problem of interest is formulated in section 2. Then we present the description of proposed methodology in section 3, which consists of the transformation induced by local parameterization and an overview of DRIPS for learning the modified system. In section 4, we test our framework on the numerical examples presented in [30], which includes linear and nonlinear dynamical systems as well as a PDE. The comparison with DNN demonstrates the efficiency and robustness of our method.

2. Problem Formulation

We consider a multi-physics system described by coupled partial differential equations (PDEs)

$$\begin{aligned} \frac{\partial s_i}{\partial t} &= \phi_i(\mathbf{s}; \gamma(\mathbf{x}, t)), \quad (\mathbf{x}, t) \in \mathcal{D} \times (0, T], \\ s_i(0) &= s_i^0, \quad i = 1, \dots, N_s, \end{aligned} \tag{2.1}$$

where the N_s state variables $\mathbf{s}(\mathbf{x}, t, \gamma(\mathbf{x}, t)) = \{s_1, \dots, s_{N_s}\}$ vary in space $\mathbf{x} \in \mathcal{D}$ and time $t \in [0, T]$ throughout the simulation domain \mathcal{D} during the simulation time interval $[0, T]$, ϕ_i are (linear/nonlinear) differential operators that contain spatial derivatives, and $\gamma(\mathbf{x}, t)$ is known time-dependent inputs. When solved numerically, the spatial domain \mathcal{D} is discretized into N_{el} elements/nodes, leading to the discretized state variable $\mathbf{S}(t; \Gamma(t))$ of (high) dimension $N_S = N_s \times N_{\text{el}}$, satisfying the following nonautonomous ordinary differential equations (ODEs) (2.2)

$$\begin{cases} \frac{d\mathbf{S}}{dt}(t) = \Phi(\mathbf{S}, \Gamma(t)), \\ \mathbf{S}(0) = \mathbf{S}_0, \end{cases} \tag{2.2}$$

where $\Gamma(t)$ is a vector-value time-dependent input known from spatial discretization of $\gamma(\mathbf{x}, t)$.

Given a set of measurement data of the state variables (elaborated in section 3.2.1), our goal is to construct a numerical surrogate model which can learn the behavior of the unknown nonautonomous system (2.2). Specifically, an accurate prediction $\hat{\mathbf{S}}$ of the true state variable \mathbf{S} (satisfying (2.2)) can be made for an arbitrary initial condition \mathbf{S}_0 and an external input process $\Gamma(t)$ within a finite time horizon $T > 0$, i.e.,

$$\hat{\mathbf{S}}(t_k; \mathbf{S}_0, \Gamma(t)) \approx \mathbf{S}(t_k; \mathbf{S}_0, \Gamma(t)), \quad k = 1, \dots, N_T, \quad 0 = t_0 < \dots < t_{N_T} = T. \quad (2.3)$$

In the following context, we take $\Gamma(t)$ as a scalar function for illustration purpose. The method can be easily applied to vector-valued time-dependent inputs component by component.

3. Methodology

In this section, we present the description of a framework for learning nonautonomous systems (2.2) using DMD. It includes two major steps: 1. decomposing the dynamical system into a modified system comprising a sequence of local systems by parameterizing the external input $\Gamma(t)$ locally in time; 2. learning the local parametric systems via DRIPS. The first step follows the same reconstruction as in [30] and the second step is adopted from the DRIPS framework proposed in our previous work [31].

3.1. Local parameterization and modified system

The corresponding discrete-time dynamical system of (2.2) is described by

$$\begin{aligned} \mathbf{S}(t_{k+1}) &= \Phi_{\Delta t}(\mathbf{S}(t_k), \Gamma(t_k)) \\ &:= \mathbf{S}(t_k) + \int_{t_k}^{t_k + \Delta t} \Phi(\mathbf{S}(\tau), \Gamma(\tau)) d\tau, \\ &= \mathbf{S}(t_k) + \int_0^{\Delta t} \Phi(\mathbf{S}(t_k + \tau), \Gamma(t_k + \tau)) d\tau, \end{aligned} \quad (3.1)$$

for the uniform time discretization $t_k = k\Delta t \in [0, T]$ with $k = 0, \dots, N_T$. In each time interval $[t_k, t_{k+1}]$, $k = 0, \dots, N_T - 1$, a local parameterization is made for the given external input function $\Gamma(t)$ in the form

$$\tilde{\Gamma}_k(\tau; \mathbf{p}_k) := \sum_{j=1}^{N_{\text{par}}} p_k^j b_j(\tau) \approx \Gamma(t_k + \tau), \quad \tau \in [0, \Delta t], \quad (3.2)$$

where $\{b_j(\tau), j = 1, \dots, N_{\text{par}}\}$ is a set of prescribed analytical basis functions and

$$\mathbf{p}_k = (p_k^1, \dots, p_k^{N_{\text{par}}}) \in \mathbb{R}^{N_{\text{par}}} \quad (3.3)$$

are the basis coefficients parameterizing the local input $\Gamma(t)$ in $[t_k, t_{k+1}]$. Examples of local parameterization of a given input $\Gamma(t)$ include interpolating polynomials, Taylor polynomials and etc. (see section 3.1 in [30]). Then a global parameterization can be constructed for the external input $\Gamma(t)$ as follows

$$\tilde{\Gamma}(t; \mathbf{p}) = \sum_{k=0}^{N_T-1} \tilde{\Gamma}_k(t - t_k; \mathbf{p}_k) \mathbb{I}_{[t_k, t_{k+1}]}(t), \quad (3.4)$$

where

$$\mathbf{p} = \{\mathbf{p}_k\}_{k=0}^{N_T-1} \in \mathbb{R}^{N_T \times N_{\text{par}}} \quad (3.5)$$

is a global parameter set for $\tilde{\Gamma}(t)$ and $\mathbb{I}_{[a,b]}$ is the indicator function

$$\mathbb{I}_{[a,b]}(t) = \begin{cases} 1 & \text{if } t \in [a, b], \\ 0 & \text{otherwise.} \end{cases} \quad (3.6)$$

A modified system corresponding to the true (unknown) system (2.2) is defined as follows:

$$\begin{cases} \frac{d\tilde{\mathbf{S}}}{dt}(t) = \Phi(\tilde{\mathbf{S}}, \tilde{\Gamma}(t; \mathbf{p})), \\ \tilde{\mathbf{S}}(0) = \mathbf{S}_0, \end{cases} \quad (3.7)$$

where $\tilde{\Gamma}(t; \mathbf{p})$ is the globally parameterized input defined in (3.4). Note that when the system input $\Gamma(t)$ is already known or given in a parametric form, i.e., $\tilde{\Gamma}(t) = \Gamma(t)$, the modified system (3.7) is equivalent to the original system (2.2). When the parameterized process $\tilde{\Gamma}(t)$ needs to be numerically constructed, the modified system (3.7) becomes an approximation to the true system (2.2). The approximation accuracy depends on the accuracy in $\tilde{\Gamma}(t) \approx \Gamma(t)$.

Following Lemma 3.1 in [30], one can show that there exists a function $\tilde{\Phi}_{\Delta t} : \mathbb{R}^{N_S} \times \mathbb{R}^{N_{\text{par}}} \rightarrow \mathbb{R}^{N_S}$, which depends on Φ , such that, for any time interval $[t_k, t_{k+1}]$, the solution of (3.7) satisfies

$$\tilde{\mathbf{S}}(t_{k+1}) = \tilde{\Phi}_{\Delta t}(\tilde{\mathbf{S}}(t_k), \mathbf{p}_k), \quad k = 0, \dots, N_T - 1, \quad (3.8)$$

where \mathbf{p}_k is the local parameter set (3.3) for the locally parameterized input $\tilde{\Gamma}_k(t)$ in (3.2).

3.2. Learning the modified systems via DRIPS

The function $\tilde{\Phi}_{\Delta t}$ in (3.8) governs the evolution of the solution of the modified system (3.7) and is the target function to learn. The difficulty in learning nonautonomous system is now shifted to the task of learning the parametric system (3.8) in any local time interval $[t_k, t_{k+1}]$. This task falls into the category of problems where DRIPS framework applies.

3.2.1. Training and testing dataset

We first elaborate on how to collect the training dataset. Given a set of known external inputs $\{\Gamma^{(i)}(t)\}_{i=1}^{N_{\text{traj}}}$ and a prescribed set of discrete time instances $0 = t_0 < t_1 < \dots < t_k < \dots < t_{N_{T^{(i)}}} = T^{(i)}$ with $\Delta t = t_{k+1} - t_k, k = 0, \dots, N_{T^{(i)}} - 1$, we assume $N_{\text{snap}}^{(k,i)}$ pairs of the input $(\mathbf{S}_j^{(i)}(t_k), \Gamma^{(i)}(t_k))$ -output $(\mathbf{S}_j^{(i)}(t_{k+1}))$ responses from the true discrete-time dynamical system (3.1) are available along the i th trajectory within the time interval $[t_k, t_{k+1}]$, i.e.,

$$\mathbf{S}_j^{(i)}(t_{k+1}) = \Phi_{\Delta t}(\mathbf{S}_j^{(i)}(t_k), \Gamma^{(i)}(t_k)), \quad j = 1, \dots, N_{\text{snap}}^{(k,i)}, \quad k = 0, \dots, N_{T^{(i)}} - 1, \quad i = 1, \dots, N_{\text{traj}}. \quad (3.9)$$

The local parameterization of $\Gamma^{(i)}(t_k)$ gives $\tilde{\Gamma}_k^{(i)}(\tau; \mathbf{p}_k^{(i)})$, where $\tau \in [0, \Delta t]$ and $\mathbf{p}_k^{(i)}$ is the parameter set for the local parameterization of the input in the form of (3.2). Now denote each local dataset as

$$\mathcal{S}_{\text{train}}^{(k,i)} = \{(\mathbf{S}_j^{(i)}(t_k), \mathbf{p}_k^{(i)}), \mathbf{S}_j^{(i)}(t_{k+1})\}, \quad j = 1, \dots, N_{\text{snap}}^{(k,i)}. \quad (3.10)$$

Notice that the following input $(\mathbf{S}_j^{(i)}(t_k), \mathbf{p}_k^{(i)})$ -output $\mathbf{S}_j^{(i)}(t_{k+1})$ responses hold approximately in the underlying modified system (3.8), i.e.,

$$\mathbf{S}_j^{(i)}(t_{k+1}) \approx \tilde{\Phi}_{\Delta t}(\mathbf{S}_j^{(i)}(t_k), \mathbf{p}_k^{(i)}), \quad j = 1, \dots, N_{\text{snap}}^{(k,i)}, \quad k = 0, \dots, N_{T^{(i)}} - 1, \quad i = 1, \dots, N_{\text{traj}}. \quad (3.11)$$

Then the full training dataset can be represented as

$$\mathcal{S}_{\text{train}} = \cup_{k,i} \mathcal{S}_{\text{train}}^{(k,i)}, \quad k = 0, \dots, N_{T^{(i)}} - 1, \quad i = 1, \dots, N_{\text{traj}}. \quad (3.12)$$

On re-ordering using a single index, the training dataset takes the form

$$\mathcal{S}_{\text{train}} = \cup_{m=1}^{N_{\text{MC}}} \mathcal{S}_{\text{train}}^{(m)}, \quad N_{\text{MC}} = \sum_{i=1}^{N_{\text{traj}}} N_{T^{(i)}}, \quad (3.13)$$

where

$$\mathcal{S}_{\text{train}}^{(m)} = \{(\mathbf{S}_j^{(m)}(0), \mathbf{p}^{(m)}), \mathbf{S}_j^{(m)}(\Delta t)\}, \quad j = 1, \dots, N_{\text{snap}}^{(m)}. \quad (3.14)$$

Our goal is to construct from this dataset $\mathcal{S}_{\text{train}}$ a surrogate model of the unknown system (3.8). This will allow us to predict the trajectory of the state variable $\mathbf{S}(t; \Gamma^*(t))$ from a different external input $\Gamma^*(t) \notin \{\Gamma^{(i)}(t)\}_{i=1}^{N_{\text{traj}}}$, i.e., $\{\mathbf{S}(t_0, \Gamma^*(t_0)), \dots, \mathbf{S}(t_{N_{T^*}}, \Gamma^*(t_{N_{T^*}}))\}$ at a low cost. The corresponding test dataset can be obtained after representing $\Gamma^*(t_k)$ by $\tilde{\Gamma}_k^*(\tau; \mathbf{p}_k^*)$ via local parameterization (3.2),

$$\mathcal{S}_{\text{test}} = \{\tilde{\mathbf{S}}(t_0, \mathbf{p}_0^*), \dots, \tilde{\mathbf{S}}(t_{N_{T^*}}, \mathbf{p}_{N_{T^*}}^*)\}. \quad (3.15)$$

The target function $\tilde{\Phi}_{\Delta t}$ and the modified system (3.8) can be learned within our DRIPS framework, which consists of the offline step and online step that are detailed in Sections 3.2.2 and 3.2.3, respectively.

3.2.2. Offline Step: DMD-Based Surrogates

For nonautonomous system (2.2), the dynamics of \mathbf{S} , i.e., the functional form of Φ in (2.2) or $\Phi_{\Delta t}$ in (3.1) is unknown. So is $\tilde{\Phi}_{\Delta t}$ in (3.8) for the modified systems. In the first step of our algorithm, we replace the unknown discrete system (3.8) with its linear surrogate model constructed from the dataset (3.13). The latter task is facilitated by the Koopman operator theory, which allows one to handle the potential nonlinearity in the unknown dynamic Φ and $\tilde{\Phi}_{\Delta t}$:

Definition 3.1 (Koopman operator [32]). *For nonlinear dynamic system (2.2), the Koopman operator $\mathcal{K}^{\Gamma(t)}$ is an infinite-dimensional linear operator that acts on all observable functions $g : \mathcal{M} \rightarrow \mathbb{C}$ so that*

$$\mathcal{K}^{\Gamma(t)}g(\mathbf{S}(t)) = g(\Phi(\mathbf{S}(t), \Gamma(t))). \quad (3.16)$$

For discrete dynamic system (3.8), the discrete-time Koopman operator $\mathcal{K}_{\Delta t}^{\mathbf{p}_k}$ is

$$\mathcal{K}_{\Delta t}^{\mathbf{p}_k}g(\mathbf{S}(t_k; \mathbf{p}_k)) = g(\tilde{\Phi}_{\Delta t}(\mathbf{S}(t_k; \mathbf{p}_k), \mathbf{p}_k)) = g(\mathbf{S}(t_{k+1}; \mathbf{p}_k)). \quad (3.17)$$

The Koopman operator transforms the finite-dimensional nonlinear problem (3.8) in the state space into the infinite-dimensional linear problem (3.17) in the observable space. Since $\mathcal{K}_{\Delta t}^{\mathbf{p}_k}$ is an infinite-dimensional linear operator, it is equipped with infinite eigenvalues $\{\lambda_i(\mathbf{p}_k)\}_{i=1}^{\infty}$ and eigenfunctions $\{\phi_i(\mathbf{p}_k)\}_{i=1}^{\infty}$. In practice, one has to make do with a finite number of the eigenvalues and eigenfunctions. The following assumption is essential to both a finite-dimensional approximation and the choice of observables.

Assumption 3.1. *Let $\mathbf{y}(t_k; \mathbf{p}_k)$ denote an $N \times 1$ vector of observables,*

$$\mathbf{y}(t_k; \mathbf{p}_k) = \mathbf{g}(\mathbf{S}(t_k; \mathbf{p}_k)) = \begin{bmatrix} g_1(\mathbf{S}(t_k; \mathbf{p}_k)) \\ \vdots \\ g_N(\mathbf{S}(t_k; \mathbf{p}_k)) \end{bmatrix}, \quad (3.18)$$

where $g_j : \mathcal{M} \rightarrow \mathbb{C}$ is an observable function with $j = 1, \dots, N$. If the chosen observables \mathbf{g} are restricted to an invariant subspace spanned by eigenfunctions of the Koopman operator $\mathcal{K}_{\Delta t}^{\mathbf{p}_k}$, then they induce a linear operator $\mathbf{K}(\mathbf{p}_k)$ that is finite-dimensional and advances these eigen-observable functions on this subspace [33].

Assumption 3.1 enables one to deploy the DMD Algorithm 1 to approximate the N -dimensional linear operator $\mathbf{K}(\mathbf{p}_k)$ and its low-dimensional approximation $\mathbf{K}_r(\mathbf{p}_k)$ of rank r . At each parameter point $\mathbf{p}_k^{(i)}$ with $k = 1, \dots, N_{T^{(i)}}$, $i = 1, \dots, N_{\text{traj}}$, the discrete system (3.11) on state space is approximated by an N -dimensional linear surrogate model

$$\mathbf{y}(t_{k+1}; \mathbf{p}_k^{(i)}) = \mathbf{K}(\mathbf{p}_k^{(i)})\mathbf{y}(t_k; \mathbf{p}_k^{(i)}) \quad (3.19)$$

on observable space. The two spaces are connected by the observable function \mathbf{g} and its inverse \mathbf{g}^{-1} . Algorithm 1 directly induces the ROM for (3.19),

$$\mathbf{y}_r(t_{k+1}; \mathbf{p}_k^{(i)}) = \mathbf{K}_r(\mathbf{p}_k^{(i)})\mathbf{y}_r(t_k; \mathbf{p}_k^{(i)}). \quad (3.20)$$

Here $\mathbf{y}_r(t_k; \mathbf{p}_k^{(i)})$ is the reduced-order observable vector or dimension r . In terms of a ROB $\mathbf{V}(\mathbf{p}_k^{(i)})$, these are expressed as

$$\mathbf{y}(t_k; \mathbf{p}_k^{(i)}) = \mathbf{V}(\mathbf{p}_k^{(i)})\mathbf{y}_r(t_k; \mathbf{p}_k^{(i)}) \quad \text{and} \quad \mathbf{K}_r(\mathbf{p}_k^{(i)}) = \mathbf{V}(\mathbf{p}_k^{(i)})^\top \mathbf{K}(\mathbf{p}_k^{(i)})\mathbf{V}(\mathbf{p}_k^{(i)}). \quad (3.21)$$

The following Algorithm 1 can be trained on the re-ordered dataset (3.13) then,

Algorithm 1: DMD algorithm on observable space [32] for parameter point $\mathbf{p}^{(m)}$, $m = 1, \dots, N_{\text{MC}}$.

Input: $\mathcal{S}_{\text{train}}^{(m)}$ in (3.14), observable function \mathbf{g}

1. Create data matrices of the observables

$$\mathbf{Y}_1(\mathbf{p}^{(m)}) = \left[\begin{array}{c|ccc} & & & \\ \mathbf{g}(\mathbf{S}_1(0; \mathbf{p}^{(m)})) & \dots & \mathbf{g}(\mathbf{S}_{N_{\text{snap}}^{(m)}}(0; \mathbf{p}^{(m)})) & \\ & & & \end{array} \right], \quad (3.22)$$

$$\mathbf{Y}_2(\mathbf{p}^{(m)}) = \left[\begin{array}{c|ccc} & & & \\ \mathbf{g}(\mathbf{S}_1(\Delta t; \mathbf{p}^{(m)})) & \dots & \mathbf{g}(\mathbf{S}_{N_{\text{snap}}^{(m)}}(\Delta t; \mathbf{p}^{(m)})) & \\ & & & \end{array} \right]. \quad (3.23)$$

2. Apply SVD $\mathbf{Y}_1(\mathbf{p}^{(m)}) \approx \mathbf{V}(\mathbf{p}^{(m)})\boldsymbol{\Sigma}(\mathbf{p}^{(m)})\mathbf{Z}(\mathbf{p}^{(m)})^*$, where $\mathbf{V}(\mathbf{p}^{(m)}) \in \mathbb{C}^{N \times r}$, $\boldsymbol{\Sigma}(\mathbf{p}^{(m)}) \in \mathbb{C}^{r \times r}$, $\mathbf{Z}(\mathbf{p}^{(m)}) \in \mathbb{C}^{r \times N_{\text{snap}}^{(m)}}$, and r is the truncation rank chosen by certain criteria and kept the same for all $m = 1, \dots, N_{\text{MC}}$.
3. Compute $\mathbf{K}_r(\mathbf{p}^{(m)}) = \mathbf{V}(\mathbf{p}^{(m)})^* \mathbf{Y}_2(\mathbf{p}^{(m)})\mathbf{Z}(\mathbf{p}^{(m)})\boldsymbol{\Sigma}(\mathbf{p}^{(m)})^{-1}$ as an $r \times r$ low-rank approximation of $\mathbf{K}(\mathbf{p}^{(m)})$.
4. Compute $\mathbf{P}^{(m_1, m_2)} = \mathbf{V}(\mathbf{p}^{(m_1)})^\top \mathbf{V}(\mathbf{p}^{(m_2)})$ for $m_1, m_2 = 1, \dots, N_{\text{MC}}$.

Output: $\mathbf{V}(\mathbf{p}^{(m)})$, $\mathbf{K}_r(\mathbf{p}^{(m)})$ and $\mathbf{P}^{(m_1, m_2)}$.

Remark 3.1. The construction of DMD surrogates can be done offline, which allows one to precompute $\mathbf{P}^{(m_1, m_2)}$ for the later online step. Although this offline step takes a majority of the computational time in the whole framework, mostly due to the computation of the high-fidelity training data (3.13), its output can be precomputed and stored efficiently; the output storage is $(N \cdot r + r \cdot r + r \cdot r \cdot (N_{\text{MC}} + 1)/2) \cdot N_{\text{MC}}$.

Remark 3.2. A theorem in [13] establishes connections between the DMD theory and the Koopman spectral analysis under specific conditions on the observables and collected data. This theorem indicates that judicious selection of the observables is critical to the success of the Koopman method. There is no principled way to select observables without expert knowledge of a dynamical system. Machine learning techniques can be deployed to identify relevant terms in the dynamics from data, which then guides the selection of the observables [1, 34]. In our numerical examples, we rely on knowledge of the underlying physics to select the observables, as was done, e.g., in [35, 36, 37, 38, 5]).

3.2.3. Online Step: Interpolation of ROBs and PROMs

For a different external input $\Gamma^*(t) \notin \{\Gamma^{(i)}(t)\}_{i=1}^{N_{\text{train}}}$, the goal is to compute $\{\mathbf{S}(t_0, \Gamma^*(t_0)), \dots, \mathbf{S}(t_{N_{T^*}}, \Gamma^*(t_{N_{T^*}}))\}$, at a low cost without evaluating (2.2). Using the same local parameterization as in (3.2), we seek to approximate the test dataset (3.15) via the PROM

$$\mathbf{y}_r(t_{k+1}; \mathbf{p}_k^*) = \mathbf{K}_r(\mathbf{p}_k^*)\mathbf{y}_r(t_k; \mathbf{p}_k^*). \quad (3.24)$$

Subsequently, the observables \mathbf{y} and the state variable \mathbf{S} are estimated as

$$\mathbf{y}(t_k; \mathbf{p}_k^*) = \mathbf{V}(\mathbf{p}_k^*) \mathbf{y}_r(t_k; \mathbf{p}_k^*), \quad \mathbf{S}(t_k; \mathbf{p}_k^*) = \mathbf{g}^{-1}(\mathbf{y}(t_k; \mathbf{p}_k^*)). \quad (3.25)$$

Therefore, the online task comprises the computation of three quantities, $\mathbf{V}(\mathbf{p}_k^*)$, $\mathbf{K}_r(\mathbf{p}_k^*)$, and $\mathbf{y}_r(t_k; \mathbf{p}_k^*)$. Notice that in general $\mathbf{p}_k^* \notin \{\mathbf{p}^{(m)}\}_{m=1}^{N_{\text{MC}}}$ for $k = 0, \dots, N_{T^*}$.

3.2.3.1 ROB Interpolation

We rely on interpolation on the Grassman manifold to compute the ROB $\mathbf{V}(\mathbf{p}_k^*)$ from the dataset $\{\mathbf{V}(\mathbf{p}^{(1)}), \dots, \mathbf{V}(\mathbf{p}^{(N_{\text{MC}})})\}$. We briefly review this interpolation approach [39] below.

Definition 3.2. *The following manifolds are of interest:*

- Grassmann manifold $\mathcal{G}(r, N)$ is the set of all subspaces in \mathbb{R}^N of dimension r ;
- Orthogonal Stiefel manifold $\mathcal{ST}(r, N)$ is the set of orthogonal ROB matrices in $\mathbb{R}^{r \times N}$.

The ROB $\mathbf{V}(\mathbf{p}^{(m)}) \in \mathbb{R}^{N \times r}$, with $m = 1, \dots, N_{\text{MC}}$ and $r \leq N$, is the full-rank column matrix, whose columns provide a basis of subspace \mathcal{S}_m of dimension r in \mathbb{R}^N . While an associated ROM is not uniquely defined by the ROB, it is uniquely defined by the subspace \mathcal{S}_m . Therefore, the correct entity to interpolate is the subspace \mathcal{S}_m , rather than the ROB $\mathbf{V}(\mathbf{p}^{(m)})$. Hence, the goal is to compute $\mathcal{S}_{k,*} = \text{range}(\mathbf{V}(\mathbf{p}_k^*))$ by interpolating between $\{\mathcal{S}_m\}_{m=1}^{N_{\text{MC}}}$ with access to the ROB $\mathbf{V}(\mathbf{p}_k^*)$.

The subspaces $\mathcal{S}_1, \dots, \mathcal{S}_{N_{\text{MC}}}$ belong to the Grassmann manifold $\mathcal{G}(r, N)$ [40, 41, 42, 43, 44]. Each r -dimensional subspace $\tilde{\mathcal{S}}$ of \mathbb{R}^N is regarded as a point of $\mathcal{G}(r, N)$ and is nonuniquely represented by a matrix $\tilde{\mathbf{V}} \in \mathbb{R}^{N \times r}$, whose columns span the subspace $\tilde{\mathcal{S}}$. The matrix $\tilde{\mathbf{V}}$ is chosen among those whose columns form a set of orthonormal vectors in \mathbb{R}^N and belong to the orthogonal Stiefel manifold $\mathcal{ST}(r, N)$ [40, 44]. There exists a projection map [40] from $\mathcal{ST}(r, N)$ onto $\mathcal{G}(r, N)$, as each matrix in $\mathcal{ST}(r, N)$ spans an r -dimensional subspace of \mathbb{R}^N and different matrices can span the same subspace. At each point $\tilde{\mathcal{S}}$ of the manifold $\mathcal{G}(r, N)$, there exists a tangent space $\mathcal{T}_{\tilde{\mathcal{S}}}$ [40, 44] of the same dimension [44]. Each point in this space is represented by a matrix $\tilde{\mathbf{M}} \in \mathbb{R}^{N \times r}$. Since $\mathcal{T}_{\tilde{\mathcal{S}}}$ is a vector space, usual interpolation is allowed for the matrices representing its points. Let $\mathbf{M}^m = m_{\mathbf{V}}(\mathbf{V}(\mathbf{p}^{(m)}))$, where $m_{\mathbf{V}}$ denotes the map from the matrix manifolds $\mathcal{G}(r, N)$ onto the tangent space $\mathcal{T}_{\tilde{\mathcal{S}}}$. This suggests a strategy of computing $\mathbf{M}^{k,*}$ via usual interpolation between $\{\mathbf{M}^m\}_{m=1}^{N_{\text{MC}}}$ and then evaluating $\mathbf{V}(\mathbf{p}_k^*)$ through the inverse map $m_{\mathbf{V}}^{-1}(\mathbf{M}^{k,*})$.

The map $m_{\mathbf{V}}$ is chosen to be the logarithmic mapping, which maps the Grassmann manifold onto its tangent space, and $m_{\mathbf{V}}^{-1}$ is chosen to be the exponential mapping, which maps the tangent space onto the Grassmann manifold itself. This choice borrows concepts of geodesic path on a Grassmann manifold from differential geometry [40, 41, 45, 46]. This strategy, discussed in detail in [39], is implemented in Algorithm 2.

Remark 3.3. The choice of the interpolation method \mathcal{P} depends on the dimension of the parameter space, N_{par} . If $N_{\text{par}} = 1$, a univariate (typically, a Lagrange type) interpolation method is chosen. Otherwise, a multivariate interpolation scheme (see, e.g., [47, 48]) is chosen.

Remark 3.4. Since the logarithmic map $\log_{\mathcal{S}_{m_0}}$ is defined in a neighborhood of $\mathcal{S}_{m_0} \in \mathcal{G}(r, N)$, the method is expected to be insensitive to the choice of the reference point \mathcal{S}_{m_0} in step 1 of Algorithm 2. This is confirmed in numerical experiments [39].

3.2.3.2 PROM Interpolation

The reduced-order operator $\mathbf{K}_r(\mathbf{p}_k^*)$ in (3.24) is computed via interpolation on the matrix manifold between the ROMs $\{\mathbf{K}_r(\mathbf{p}^{(1)}), \dots, \mathbf{K}_r(\mathbf{p}^{(N_{\text{MC}})})\}$. This is done in two steps [49]:

- Step A). Since any ROM can be endowed with multiple alternative ROBs, the resulting ROMs may have been computed in different generalized coordinates system. The validity of an interpolation may crucially depend on the choice of the representative element within each equivalent class.

Algorithm 2: Interpolation of ROBs [39]

Input: $\{\mathbf{V}(\mathbf{p}^{(m)})\}_{m=1}^{N_{MC}}$, $\{\mathbf{P}^{(m_1, m_2)}\}_{m_1, m_2=1}^{N_{MC}}$, $\{\mathbf{p}^{(m)}\}_{m=1}^{N_{MC}}$ and target parameter point $\{\mathbf{p}_k^*\}_{k=0}^{N_{T^*}}$

1. Denote $\mathcal{S}_m = \text{range}(\mathbf{V}(\mathbf{p}^{(m)}))$, for $m = 1, \dots, N_{MC}$. A point \mathcal{S}_{m_0} with $m_0 \in \{1, \dots, N_{MC}\}$ of the manifold is chosen as a reference and origin point for interpolation.
2. Select points \mathcal{S}_m with $m \in \mathcal{I}_{m_0} \subset \{1, \dots, N_{MC}\}$, which lie in a sufficiently small neighborhood of \mathcal{S}_{m_0} , and use the logarithm map $\log_{\mathcal{S}_{m_0}}$ to map $\{\mathcal{S}_m\}_{m \in \mathcal{I}_{m_0}}$ onto matrices $\{\mathbf{M}^m\}_{m \in \mathcal{I}_{m_0}}$ representing the corresponding points of $\mathcal{T}_{\mathcal{S}_{m_0}}$. This is computed as

$$\begin{aligned} (\mathbf{I} - \mathbf{V}(\mathbf{p}^{(m_0)})\mathbf{V}(\mathbf{p}^{(m_0)})^\top)\mathbf{V}(\mathbf{p}^{(m)})(\mathbf{P}^{(m_0, m)})^{-1} &= \mathbf{U}_m \boldsymbol{\Omega}_m \mathbf{W}_m^\top, \quad (\text{thin SVD}) \\ \mathbf{M}^m &= \mathbf{U}_m \tan^{-1}(\boldsymbol{\Omega}_m) \mathbf{W}_m^\top. \end{aligned} \quad (3.26)$$

3. Compute $\mathbf{M}^{k,*}$ by interpolating $\{\mathbf{M}^m\}_{m \in \mathcal{I}_{m_0}}$ entry by entry:

$$M_{ij}^{k,*} = \mathcal{P}(\mathbf{p}_k^*; \{M_{ij}^m, \mathbf{p}^{(m)}\}_{m \in \mathcal{I}_{m_0}}), \quad i = 1, \dots, N, \quad j = 1, \dots, r. \quad (3.27)$$

4. Use the exponential map $\exp_{\mathcal{S}_{m_0}}$ to map the matrix $\mathbf{M}^{k,*}$, representing a point of $\mathcal{T}_{\mathcal{S}_{m_0}}$, onto the desired subspace $\mathcal{S}_{k,*}$ on $\mathcal{G}(r, N)$ spanned by the ROB $\mathbf{V}(\mathbf{p}_k^*)$. This is computed as

$$\begin{aligned} \mathbf{M}^{k,*} &= \mathbf{U}_{k,*} \tan^{-1}(\boldsymbol{\Omega}_{k,*}) \mathbf{W}_{k,*}^\top, \quad (\text{thin SVD}) \\ \mathbf{V}(\mathbf{p}_k^*) &= \mathbf{V}(\mathbf{p}^{(m_0)}) \mathbf{W}_{k,*} \cos(\boldsymbol{\Omega}_{k,*}) + \mathbf{U}_{k,*} \sin(\boldsymbol{\Omega}_{k,*}). \end{aligned} \quad (3.28)$$

Output: $\{\mathbf{V}(\mathbf{p}_k^*)\}_{k=1}^{N_{T^*}}$

Given the precomputed ROMs $\{\mathbf{K}_r(\mathbf{p}^{(1)}), \dots, \mathbf{K}_r(\mathbf{p}^{(N_{MC})})\}$, a set of congruence transformations is determined so that a representative element of the equivalent ROBs for each precomputed ROM is chosen to assign the precomputed ROMs into consistent sets of generalized coordinates. The consistency is enforced by solving the orthogonal Procrustes problems [50],

$$\min_{\mathbf{S}_m, \mathbf{S}_m^\top \mathbf{S}_m = \mathbf{I}_r} \|\mathbf{V}(\mathbf{p}^{(m)})^\top \mathbf{S}_m - \mathbf{V}(\mathbf{p}^{(m_0)})\|_F, \quad \forall m = 1, \dots, N_{MC}, \quad (3.29)$$

where $m_0 \in \{1, \dots, N_{MC}\}$ is chosen as a reference configuration. The representative element is identified by solving the above problem analytically. This procedure is summarized in Algorithm 3.

Algorithm 3: Step A of the PROM interpolation [39]

Input: $\{\mathbf{K}_r(\mathbf{p}^{(1)}), \dots, \mathbf{K}_r(\mathbf{p}^{(N_{MC})})\}$, $\{\mathbf{P}^{(i,j)}\}_{m_1, m_2=1}^{N_{MC}}$, reference configuration choice m_0

For $m \in \{1, \dots, N_{MC}\} \setminus \{m_0\}$

– Compute $\mathbf{P}^{(m, m_0)} = \mathbf{U}_{m, m_0} \boldsymbol{\Sigma}_{m, m_0} \mathbf{Z}_{m, m_0}^\top$ (SVD),

– Compute $\mathbf{S}_m = \mathbf{U}_{m, m_0} \mathbf{Z}_{m, m_0}^\top$,

– Transform $\tilde{\mathbf{K}}_r(\mathbf{p}^{(m)}) = \mathbf{S}_m^\top \mathbf{K}_r(\mathbf{p}^{(m)}) \mathbf{S}_m$

End

Output: $\{\tilde{\mathbf{K}}_r(\mathbf{p}^{(1)}), \dots, \tilde{\mathbf{K}}_r(\mathbf{p}^{(N_{MC})})\}$

Remark 3.5. An optimal choice of the reference configuration m_0 , if it exists, remains an open problem.

Remark 3.6. Step A is related to mode-tracking procedures based on the modal assurance criterion (MAC) [51]. This connection is illucidated in [49].

- Step B). The transformed ROMs $\{\tilde{\mathbf{K}}_r(\mathbf{p}^{(1)}), \dots, \tilde{\mathbf{K}}_r(\mathbf{p}^{(N_{\text{MC}})})\}$ are interpolated to compute ROMs $\{\mathbf{K}_r(\mathbf{p}_k^*)\}_{k=1}^{N_{T^*}}$. Similar to Section 3.2.3.1, this interpolation must be performed on a specific manifold containing both $\{\tilde{\mathbf{K}}_r(\mathbf{p}^{(1)}), \dots, \tilde{\mathbf{K}}_r(\mathbf{p}^{(N_{\text{MC}})})\}$ and $\{\mathbf{K}_r(\mathbf{p}_k^*)\}_{k=1}^{N_{T^*}}$, so that the distinctive properties (e.g., orthogonality, nonsingularity) are preserved. The main idea again is to first map all the precomputed matrices onto the tangent space to the matrix manifold of interest at a chosen reference point using the logarithm mapping, then interpolate the mapped data in this linear vector space, and finally map the interpolated result back onto the manifold of interest using the associated exponential map. This is done in Algorithm 4.

Algorithm 4: Step B of the PROM interpolation [39]

Input: $\{\tilde{\mathbf{K}}_r(\mathbf{p}^{(1)}), \dots, \tilde{\mathbf{K}}_r(\mathbf{p}^{(N_{\text{MC}})})\}$, reference configuration choice m_0

1. **For** $m \in \{1, \dots, N_{\text{MC}}\} \setminus \{m_0\}$

– Compute $\mathbf{M}^m = \log_{\tilde{\mathbf{K}}_r(\mathbf{p}^{(m_0)})}(\tilde{\mathbf{K}}_r(\mathbf{p}^{(m)}))$

End

2. Compute $\mathbf{M}^{k,*}$ by interpolating $\{\mathbf{M}^m\}_{m \in \mathcal{I}_{m_0}}$ entry by entry, as in (3.27)

3. Compute $\mathbf{K}_r(\mathbf{p}_k^*) = \exp_{\tilde{\mathbf{K}}_r(\mathbf{p}^{(m_0)})}(\mathbf{M}^{k,*})$

Output: $\{\mathbf{K}_r(\mathbf{p}_k^*)\}_{k=1}^{N_{T^*}}$

Remark 3.7. The log and exp in Algorithm 4 denote the matrix logarithm and exponential respectively. The specific expressions of different matrix manifolds of interest are listed in Table 4.1 of [49].

3.2.3.3 Computation of the Solution

With $\{\mathbf{K}_r(\mathbf{p}_k^*)\}_{k=0}^{N_{T^*}}$ and $\{\mathbf{V}(\mathbf{p}_k^*)\}_{k=0}^{N_{T^*}}$ computed, we use (3.24) and (3.25) to obtain the solution.

3.2.4. Algorithm Summary

The proposed framework is implemented in Algorithm 5.

Algorithm 5: Learning nonautonomous system via DMD

Offline Step:

For $m = 1, \dots, N_{\text{MC}}$,

Get the training data (3.13),

Input: $\mathcal{S}_{\text{train}}^{(m)}$ and $\mathbf{g} \xrightarrow{\text{Algorithm 1}}$ Output: $\mathbf{V}(\mathbf{p}^{(m)})$, $\mathbf{K}_r(\mathbf{p}^{(m)})$ and $\mathbf{P}^{(m_1, m_2)}$

End

Online Step:

- Interpolation of ROBs:

Input: $\{\mathbf{V}(\mathbf{p}^{(m)})\}_{m=1}^{N_{\text{MC}}}$, $\{\mathbf{P}^{(m_1, m_2)}\}_{m_1, m_2=1}^{N_{\text{MC}}}$, $\{\mathbf{p}^{(m)}\}_{m=1}^{N_{\text{MC}}}$, $\{\mathbf{p}_k^*\}_{k=0}^{N_{T^*}} \xrightarrow{\text{Algorithm 2}}$ Output: $\{\mathbf{V}(\mathbf{p}_k^*)\}_{k=1}^{N_{T^*}}$

- Interpolation of PROMs:

Input: $\{\mathbf{K}_r(\mathbf{p}^{(m)})\}_{m=1}^{N_{\text{MC}}}$, $\{\mathbf{P}^{(m_1, m_2)}\}_{m_1, m_2=1}^{N_{\text{MC}}}$, reference choice $m_0 \xrightarrow{\text{Algorithms 3 \& 4}}$ Output: $\mathbf{K}_r(\mathbf{p}_k^*)$

- DMD reconstruction:

Input: $\mathbf{K}_r(\mathbf{p}_k^*)$, $\mathbf{V}(\mathbf{p}_k^*)$, $\mathbf{y}(t = 0; \mathbf{p}_0^*)$, $\mathbf{g} \xrightarrow{(3.24), (3.25)}$ Output: $\mathbf{S}_{\text{DMD}}(t_k; \mathbf{p}_k^*)$

Remark 3.8. The sampling strategy for $\{\mathbf{p}^{(1)}, \dots, \mathbf{p}^{(N_{\text{MC}})}\}$ in the parameter space plays a key role in the accuracy of the subspace approximation. The so-called “curse of dimensionality”, i.e., the number of training samples N_{MC} needed grows exponentially with the number of parameters, N_{par} , is a well-known challenge. In general, uniform sampling is used for $N_{\text{par}} \leq 5$ and moderately computationally intensive HFMs, latin hypercube sampling is used for $N_{\text{par}} > 5$ and moderately computationally intensive HFMs, and adaptive, goal-oriented, greedy sampling is used for $N_{\text{par}} > 5$ and highly computationally intensive HFMs. We limit our numerical experiments to $N_{\text{par}} = 3$ for simplicity, leaving the challenge posed by the curse of dimensionality for future studies.

4. Numerical Experiments

In this section, we tested our proposed framework on every numerical example presented in [30]. Synthetic data generated from known dynamical systems with known time-dependent inputs is employed to validate the proposed framework. The training data are generated by solving the known system with a high-resolution numerical scheme in Matlab, e.g., *ode45*, which is based on an explicit fourth-order Runge-Kutta formula. In all the following examples, the inputs are parameterized locally the same way as in [30], i.e., by interpolating polynomials over equally spaced points. Other parameterization strategies produce similar results and thus not included here for brevity.

For the convenience, we generate the training dataset in the form of (3.13) with $N_T^{(i)} \equiv 1$ for $i = 1, \dots, N_{\text{traj}}$, i.e., each trajectory only contains two data points and $N_{\text{MC}} = N_{\text{traj}}$. For each subset $\mathcal{S}_{\text{train}}^m$, the first data entry is randomly sampled from a domain $I_{\mathbf{S}}$ using uniform distribution. The second data entry is produced by solving the underlying reference dynamical system with a time step Δt and subject to a parameterized external input in the form of (3.2). We take $\Delta t = 0.1$ in all numerical examples except when other values are specified. For simplicity, we take the same number of snapshots/data pairs in each parameter point, i.e., $N_{\text{snap}}^{(m)} = N_{\text{snap}}$ for all m . Instead of uniformly sampling the parameters (3.3) as in [30], we take the parameter values on the Cartesian grid of the N_{par} -dimensional parameter space with 3 points (two endpoints and one middle point) in each dimension, i.e., $N_{\text{MC}} = N_{\text{traj}} = 3^{N_{\text{par}}}$. Therefore, the total amount of training data is $N_{\text{snap}} \times 3^{N_{\text{par}}}$ pairs in the form of (3.14). This number will be

specified in each numerical example and we see that it is much smaller than what is needed in training a neural network ($O(10^5)$ in [30]).

The sampling domain I_S and parameter domain I_P are determined by prior knowledge of the underlying unknown equations to ensure the range of the target trajectories are covered by I_S for parameters in I_P so that the assumptions in the theoretical analysis of [30] are satisfied. The same I_S and I_P are adopted from [30] and are specified separately for each example.

Our proposed learning algorithm 5 is then applied to the training dataset. The observable \mathbf{g} is determined by the underlying system and will be specified in each numerical example. Notice that the choice of observables may not be unique and optimal. Therefore, we consider the optimal construction of observables out of the scope of this paper and employ several standard tricks in DMD studies to construct reasonable observables. Once the learned model is constructed, we conduct system prediction iteratively using the model with new initial conditions and new external inputs. The prediction results are then compared with the reference solution obtained by solving the exact system with the same new inputs.

4.1. Linear scalar equation with source

We first consider the following scalar equation

$$\frac{dS}{dt} = -\alpha(t)S + \beta(t), \quad (4.1)$$

where the time-dependent inputs $\alpha(t)$ and $\beta(t)$ are locally parameterized with polynomials of degree 2. As a result, the local parameter set (3.3) $\mathbf{p}_k \in \mathbb{R}^{N_{\text{par}}}$ with $N_{\text{par}} = 3 + 3 = 6$. The training data are generated from $N_{\text{MC}} = N_{\text{traj}} = 3^6$ parameter points on the Cartesian grid of the parameter space $I_P = [-5, 5]^6$. On each parameter point $\mathbf{p}^{(m)}$, $N_{\text{snap}}^{(m)} = N_{\text{snap}} = 2$ pairs of data in the form of (3.14) are generated with $S_j^{(m)}(0)$ randomly sampled from state variable space $I_S = [-2, 2]$. The total number of data pairs is 1458 in this case.

Since S is a scalar, the observable \mathbf{g} can be designed to construct an augmented data matrix. Our choice of the observable is $\mathbf{y}(t_k; \mathbf{p}_k) = \mathbf{g}(S(t_k; \mathbf{p}_k)) = [S(t_k; \mathbf{p}_k), S(t_k; \mathbf{p}_k)^2]^\top$. Alternatively, one can construct the shift-stacked data matrices as introduced in [13]. After the DMD surrogate model is trained, we use it to conduct system prediction. In Figure 1, the prediction result with a new initial condition $S_0 = 2$ and new external inputs $\alpha(t) = \sin(4t) + 1$ and $\beta(t) = \cos(t^2/1000)$ is shown for time up to $T = 100$. The reference solution is also shown for comparison. It can be seen that our surrogate model produces accurate prediction for this relatively long-term integration.

Figure 1(b) plots errors in predictions of (4.1) learned using different values of Δt , which exhibit a different behavior than DNN as reported in Figure 4.1 of [30]. Following the same analysis as conducted in Theorem 3.5 of [30], the error of our method can be identified from two sources: 1. the approximation error of the parameterization, i.e., the difference between the true non-autonomous system (2.2) and the modified system (3.7); 2. the error of the surrogate, i.e., the difference between the modified system (3.7) and the surrogate model ((3.24) and (3.25) in our DMD method). The impacts of the two sources are well balanced in DNN so the overall error stays the same order for all choices of Δt . However, the second source of error is more dominant in DMD and thus the overall error shows sensitive dependence on the choice of Δt . It is well reported in the literature of DMD studies that the surrogate accuracy is highly dependent on the number of snapshots N_{snap} , sampling frequency (i.e., $1/\Delta t$) and the underlying system itself.

4.2. Predator-prey model with control

We now consider the following Lotka-Volterra predator-prey model with a time-dependent input $u(t)$:

$$\begin{aligned} \frac{dS_1}{dt} &= S_1 - S_1 S_2 + u(t), \\ \frac{dS_2}{dt} &= -S_2 + S_1 S_2. \end{aligned} \quad (4.2)$$

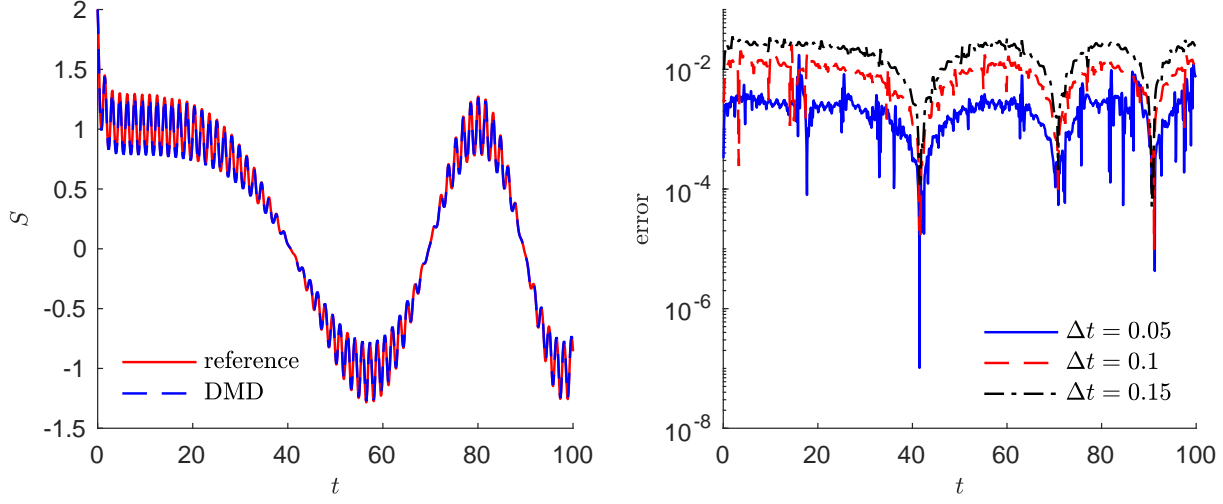


Figure 1: (a). DMD prediction of (4.1) with inputs $\alpha(t) = \sin(4t) + 1$ and $\beta(t) = \cos(t^2/1000)$; (b). The difference between the DMD surrogate and the reference solution using different Δt .

The local parameterization for the external input is conducted using quadratic polynomials, i.e., $\mathbf{p} \in \mathbb{R}^3$. We set $I_{\mathbf{p}} = [0, 5]^3$ and the state variable space $I_{\mathbf{S}} = [0, 5]^2$. Therefore, $N_{\text{MC}} = N_{\text{traj}} = 27$ parameter points on the Cartesian grid of $I_{\mathbf{p}}$ are selected to generate the training data with $N_{\text{snap}} = 9$ pairs. The total number of training data pairs is 243. The observable is constructed in the following way:

$$\mathbf{y}(t_k; \mathbf{p}_k) = \mathbf{g}(\mathbf{S}(t_k; \mathbf{p}_k)) = [S_1(t_k; \mathbf{p}_k), S_2(t_k; \mathbf{p}_k), S_1(t_k; \mathbf{p}_k)^2, S_1(t_k; \mathbf{p}_k)S_2(t_k; \mathbf{p}_k), S_2(t_k; \mathbf{p}_k)^2, S_1(t_k; \mathbf{p}_k)^3, S_1(t_k; \mathbf{p}_k)^2S_2(t_k; \mathbf{p}_k), S_1(t_k; \mathbf{p}_k)S_2(t_k; \mathbf{p}_k)^2, S_2(t_k; \mathbf{p}_k)^3]^\top$$

The trained DMD surrogate is tested with external input $u(t) = \sin(t/3) + \cos(t) + 2$ and initial condition $\mathbf{S}_0 = [3, 2]$ for time up to $T = 100$. Figure 2 shows the prediction profile and accuracy for S_1 compared with reference solution. The accuracy is satisfactory for this relatively long-time prediction. Similar results hold for S_2 .

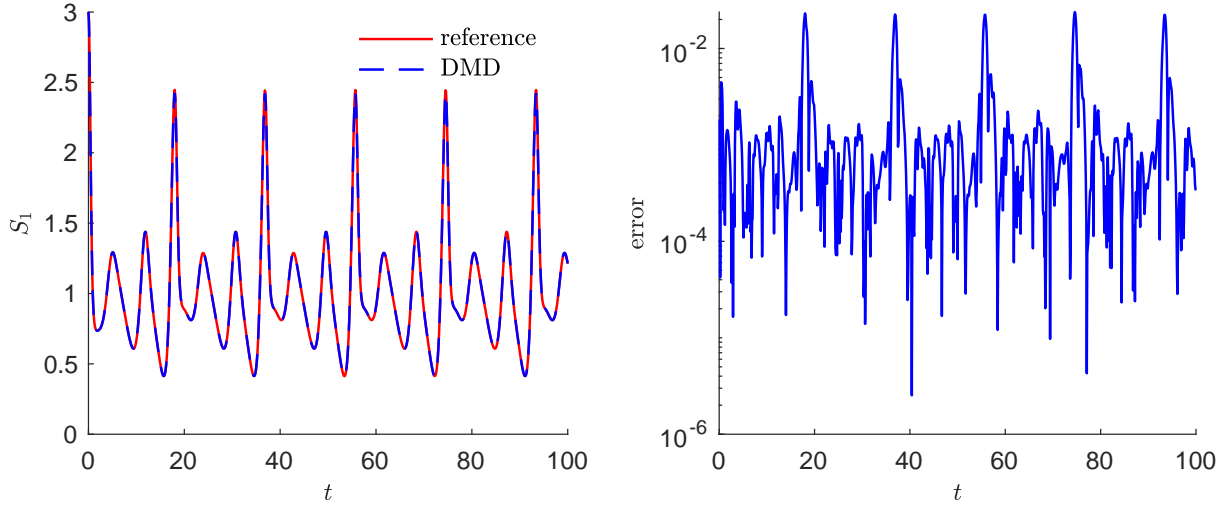


Figure 2: DMD prediction of (4.2) with inputs $u(t) = \sin(t/3) + \cos(t) + 2$ and $(S_1(0), S_2(0)) = (3, 2)$. Left: S_1 solution profile; Right: Absolute error of S_1 .

4.3. Forced Oscillator

We then consider a forced oscillator

$$\begin{aligned}\frac{dS_1}{dt} &= S_2, \\ \frac{dS_2}{dt} &= -\nu(t)S_1 - S_2 + f(t),\end{aligned}\tag{4.3}$$

where the damping term $\nu(t)$ and the forcing $f(t)$ are time-dependent processes. Local parameterization for the inputs is conducted using quadratic polynomials and $N_{\text{MC}} = N_{\text{traj}} = 3^6$ parameter points on the Cartesian grid of $I_{\mathbf{p}} = [-1, 1]^6$ are selected for training. On each parameter point, initial conditions are sampled randomly from state variable space $I_{\mathbf{S}} = [-3, 3]^2$ and $N_{\text{snap}} = 3$ pairs of one-time step input-output data pairs are collected, making a total number of 2187 pairs of training data.

Predictions using the trained DMD model is shown in Figure 3 for an arbitrarily chosen external inputs $\nu(t) = \cos(t)$ and $f(t) = t/200$. We observe very good agreement with the reference solution for relatively long-term simulation up to $T = 100$. Moreover, when $t > 80$, the value of x_1 has been out of the training domain $I_{\mathbf{S}} = [-3, 3]$, whereas the DMD model still generates accurate predictions. This shows some generalization ability of the DMD model.

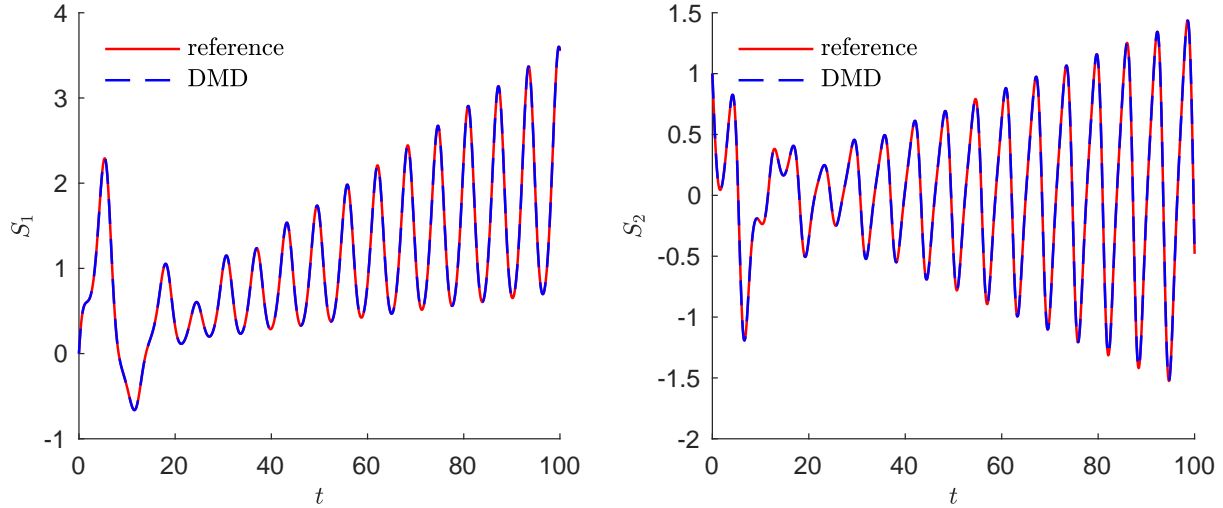


Figure 3: DMD prediction of (4.3) with inputs $\nu(t) = \cos(t)$ and $f(t) = t/200$.

4.4. 1D PDE: heat equation with source

We now consider a PDE model, in particular, the following heat equation with a source term,

$$\begin{aligned}s_t &= s_{xx} + q(t, x), \quad x \in [0, 1], \\ s(0, x) &= s_0(x), \\ s(t, 0) &= s(t, 1) = 0,\end{aligned}\tag{4.4}$$

where $q(t, x)$ is the source term varying in both space and time. We set the source term to be

$$q(t, x) = \alpha(t)e^{-\frac{(x-\mu)^2}{\sigma^2}}\tag{4.5}$$

where $\alpha(t)$ is its time-varying amplitude and parameters μ and σ determine its spatial profile.

The learning of (4.4) is conducted in a discrete space. $N_S = 20$ equally distributed grid points are employed in the domain $[0, 1]$. Let

$$\mathbf{S}(t) = [s(t, x_1), \dots, s(t, x_{N_S})]^\top.\tag{4.6}$$

Local parameterization of the input $\alpha(t)$ is conducted using 4th order polynomials. More specifically, $N_{\text{MC}} = N_{\text{traj}} = 3^7$ parameter points are selected from the Cartesian grid of the local parameterization space $I_{\mathbf{p}} = I_{\alpha} \times I_{\mu} \times I_{\sigma} = [0, 1]^5 \times [0, 3] \times [0.05, 0.5]$ and $N_{\text{snap}} = 25$ training data pairs are generated by randomly sampling from state variable space $I_{\mathbf{S}} = [0, 1]^{N_S}$ and doing one-time step simulation. There are 54675 pairs of data in the training dataset. Then we test the prediction ability of our surrogate model for a new source term (not in training data set), where $\alpha = t - \lfloor t \rfloor$ is a sawtooth discontinuous function, $\mu = 1$ and $\sigma = 0.5$.

The prediction results are shown in Figure 4 along with the reference solution solved from the underlying PDE. We observe satisfactory agreement between the surrogate model prediction to the reference

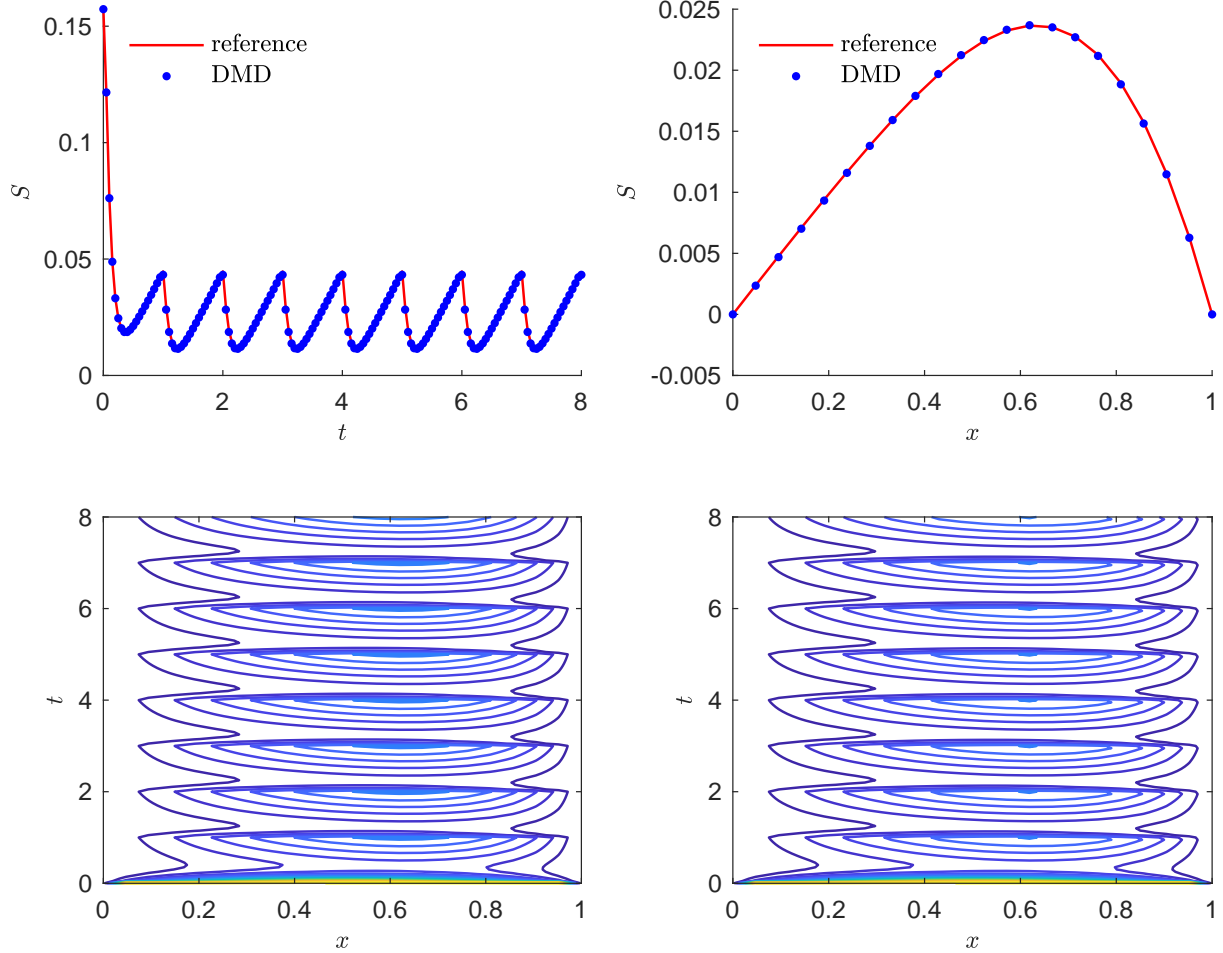


Figure 4: DMD prediction of (4.4) with inputs $\alpha(t) = t - \lfloor t \rfloor$, $\mu = 1$ and $\sigma = 0.5$. (a). Solution evolution at $x = 5$; (b). Solution profile at $t = 2$; (c). Reference solution contours over time; (d). DMD prediction contours over time.

5. Conclusion

In this paper, we presented a numerical framework for learning unknown nonautonomous dynamical systems via DMD. To circumvent the numerical difficulties of computing the spectrum of the nonautonomous Koopman operator, the nonautonomous system is transformed into a family of modified systems over a set of discrete time instances. The modified system, induced by a local parameterization of the external time-dependent inputs over each time instance, can be learned via our previous work dimension

reduction and interpolation for parametric systems (DRIPS). The interpolation of the surrogate models in the parameter space allows one to conduct system predictions for other external time-dependent inputs by computing the parametric ROM of the new modified system iteratively over each time instance. The advantages of our proposed framework include: 1. Unlike previous work of approximating the spectrum of the time-dependent Koopman operator, our method works for general nonautonomous systems without any special requirements in special structures (e.g. periodic/quasi periodic). 2. Compared with other data-driven learning method like DNN, our method can achieve comparably satisfactory accuracy using much less training data. The efficiency and robustness of our method are demonstrated by various numerical examples of ODEs and PDEs. Future work along this line of research includes application of this framework to more complex large systems and rigorous analysis for the surrogate modeling errors.

References

- [1] M. Schmidt, H. Lipson, Distilling free-form natural laws from experimental data, *Science* 324 (5923) (2009) 81–85.
- [2] H. Schaeffer, Learning partial differential equations via data discovery and sparse optimization, *Proceedings of the Royal Society A: Mathematical, Physical and Engineering Sciences* 473 (2197) (2017) 20160446.
- [3] S. L. Brunton, J. L. Proctor, J. N. Kutz, Discovering governing equations from data by sparse identification of nonlinear dynamical systems, *Proceedings of the National Academy of Sciences* 113 (15) (2016) 3932–3937.
- [4] M. Raissi, P. Perdikaris, G. E. Karniadakis, Machine learning of linear differential equations using gaussian processes, *Journal of Computational Physics* 348 (2017) 683–693.
- [5] Q. Li, F. Dietrich, E. M. Bollt, I. G. Kevrekidis, Extended dynamic mode decomposition with dictionary learning: A data-driven adaptive spectral decomposition of the koopman operator, *Chaos: An Interdisciplinary Journal of Nonlinear Science* 27 (10) (2017) 103111.
- [6] M. Korda, I. Mezić, On convergence of extended dynamic mode decomposition to the koopman operator, *Journal of Nonlinear Science* 28 (2) (2018) 687–710.
- [7] M. O. Williams, I. G. Kevrekidis, C. W. Rowley, A data-driven approximation of the koopman operator: Extending dynamic mode decomposition, *Journal of Nonlinear Science* 25 (6) (2015) 1307–1346.
- [8] R. Rico-Martinez, I. G. Kevrekidis, Continuous time modeling of nonlinear systems: A neural network-based approach, in: *IEEE International Conference on Neural Networks, IEEE, 1993*, pp. 1522–1525.
- [9] M. Raissi, Deep hidden physics models: Deep learning of nonlinear partial differential equations, *The Journal of Machine Learning Research* 19 (1) (2018) 932–955.
- [10] S. H. Rudy, J. N. Kutz, S. L. Brunton, Deep learning of dynamics and signal-noise decomposition with time-stepping constraints, *Journal of Computational Physics* 396 (2019) 483–506.
- [11] J. Bakarji, D. M. Tartakovsky, Data-driven discovery of coarse-grained equations, *Journal of Computational Physics* 434 (2021) 110219.
- [12] P. J. Schmid, Dynamic mode decomposition of numerical and experimental data, *Journal of Fluid Mechanics* 656 (2010) 5–28.
- [13] J. H. Tu, Dynamic mode decomposition: Theory and applications, Ph.D. thesis, Princeton University (2013).

- [14] B. O. Koopman, Hamiltonian systems and transformation in hilbert space, *Proceedings of the National Academy of Sciences* 17 (5) (1931) 315–318.
- [15] S. L. Brunton, B. W. Brunton, J. L. Proctor, E. Kaiser, J. N. Kutz, Chaos as an intermittently forced linear system, *Nature communications* 8 (1) (2017) 1–9.
- [16] T. Qin, K. Wu, D. Xiu, Data driven governing equations approximation using deep neural networks, *Journal of Computational Physics* 395 (2019) 620–635.
- [17] M. Raissi, P. Perdikaris, G. E. Karniadakis, Physics-informed neural networks: A deep learning framework for solving forward and inverse problems involving nonlinear partial differential equations, *Journal of Computational Physics* 378 (2019) 686–707.
- [18] Z. Long, Y. Lu, B. Dong, Pde-net 2.0: Learning pdes from data with a numeric-symbolic hybrid deep network, *Journal of Computational Physics* 399 (2019) 108925.
- [19] K. Wu, D. Xiu, Data-driven deep learning of partial differential equations in modal space, *Journal of Computational Physics* 408 (2020) 109307.
- [20] J. L. Proctor, S. L. Brunton, J. N. Kutz, Dynamic mode decomposition with control, *SIAM Journal on Applied Dynamical Systems* 15 (1) (2016) 142–161.
- [21] J. L. Proctor, S. L. Brunton, J. N. Kutz, Generalizing koopman theory to allow for inputs and control, *SIAM Journal on Applied Dynamical Systems* 17 (1) (2018) 909–930.
- [22] J. L. Proctor, S. L. Brunton, J. N. Kutz, Including inputs and control within equation-free architectures for complex systems, *The European Physical Journal Special Topics* 225 (2016) 2413–2434.
- [23] S. L. Brunton, J. L. Proctor, J. N. Kutz, Sparse identification of nonlinear dynamics with control (sindyc), *IFAC-PapersOnLine* 49 (18) (2016) 710–715.
- [24] I. Mezic, A. Surana, Koopman mode decomposition for periodic/quasi-periodic time dependence, *IFAC-PapersOnLine* 49 (18) (2016) 690–697.
- [25] J. N. Kutz, X. Fu, S. L. Brunton, Multiresolution dynamic mode decomposition, *SIAM Journal on Applied Dynamical Systems* 15 (2) (2016) 713–735.
- [26] D. Giannakis, Data-driven spectral decomposition and forecasting of ergodic dynamical systems, *Applied and Computational Harmonic Analysis* 47 (2) (2019) 338–396.
- [27] S. Das, D. Giannakis, Delay-coordinate maps and the spectra of koopman operators, *Journal of Statistical Physics* 175 (6) (2019) 1107–1145.
- [28] H. Zhang, C. W. Rowley, E. A. Deem, L. N. Cattafesta, Online dynamic mode decomposition for time-varying systems, *SIAM Journal on Applied Dynamical Systems* 18 (3) (2019) 1586–1609.
- [29] S. Macesic, N. Crnjaric-Zic, I. Mezic, Koopman operator family spectrum for nonautonomous systems, *SIAM Journal on Applied Dynamical Systems* 17 (4) (2018) 2478–2515.
- [30] T. Qin, Z. Chen, J. D. Jakeman, D. Xiu, Data-driven learning of nonautonomous systems, *SIAM Journal on Scientific Computing* 43 (3) (2021) A1607–A1624.
- [31] H. Lu, D. M. Tartakovsky, Drips: A framework for dimension reduction and interpolation in parameter space, Available at SSRN 4196496 (2022).
- [32] J. N. Kutz, S. L. Brunton, B. W. Brunton, J. L. Proctor, Dynamic mode decomposition: data-driven modeling of complex systems, SIAM, 2016.

- [33] S. L. Brunton, B. W. Brunton, J. L. Proctor, J. N. Kutz, Koopman invariant subspaces and finite linear representations of nonlinear dynamical systems for control, *PloS One* 11 (2) (2016) e0150171.
- [34] W.-X. Wang, R. Yang, Y.-C. Lai, V. Kovanis, C. Grebogi, Predicting catastrophes in nonlinear dynamical systems by compressive sensing, *Physical Review Letters* 106 (15) (2011) 154101.
- [35] H. Lu, D. M. Tartakovsky, Lagrangian dynamic mode decomposition for construction of reduced-order models of advection-dominated phenomena, *J. Comput. Phys.* (2020) 109229.
- [36] H. Lu, D. M. Tartakovsky, Prediction accuracy of dynamic mode decomposition, *SIAM Journal on Scientific Computing* 42 (3) (2020) A1639–A1662.
- [37] H. Lu, D. M. Tartakovsky, Dynamic mode decomposition for construction of reduced-order models of hyperbolic problems with shocks, *Journal of Machine Learning for Modeling and Computing* 2 (1) (2021).
- [38] H. Lu, D. M. Tartakovsky, Extended dynamic mode decomposition for inhomogeneous problems, *Journal of Computational Physics* 444 (2021) 110550.
- [39] D. Amsallem, C. Farhat, Interpolation method for adapting reduced-order models and application to aeroelasticity, *AIAA Journal* 46 (7) (2008) 1803–1813.
- [40] P.-A. Absil, R. Mahony, R. Sepulchre, Riemannian geometry of Grassmann manifolds with a view on algorithmic computation, *Acta Applicandae Mathematica* 80 (2) (2004) 199–220.
- [41] W. M. Boothby, W. M. Boothby, *An introduction to differentiable manifolds and Riemannian geometry*, Revised, Vol. 120, Gulf Professional Publishing, 2003.
- [42] S. Helgason, *Differential geometry, Lie groups, and symmetric spaces*. ams, Graduate Texts in Mathematics (2001).
- [43] I. U. Rahman, I. Drori, V. C. Stodden, D. L. Donoho, P. Schröder, Multiscale representations for manifold-valued data, *Multiscale Modeling & Simulation* 4 (4) (2005) 1201–1232.
- [44] A. Edelman, T. A. Arias, S. T. Smith, The geometry of algorithms with orthogonality constraints, *SIAM Journal on Matrix Analysis and Applications* 20 (2) (1998) 303–353.
- [45] R. M. Wald, *General relativity* (book), Chicago, University of Chicago Press, 1984, 504 p (1984).
- [46] M. P. Do Carmo, J. Flaherty Francis, *Riemannian geometry*, Vol. 6, Springer, 1992.
- [47] H. Späth, *One dimensional spline interpolation algorithms*, AK Peters/CRC Press, 1995.
- [48] C. De Boor, A. Ron, Computational aspects of polynomial interpolation in several variables, *Mathematics of Computation* 58 (198) (1992) 705–727.
- [49] D. Amsallem, C. Farhat, An online method for interpolating linear parametric reduced-order models, *SIAM Journal on Scientific Computing* 33 (5) (2011) 2169–2198.
- [50] C. F. Van Loan, G. Golub, *Matrix computations* (johns hopkins studies in mathematical sciences), Matrix Computations (1996).
- [51] D. J. Ewins, *Modal testing: theory, practice and application*, John Wiley & Sons, 2009.